Eur. Phys. J. D **25**, 103–111 (2003)
DOI: 10.1140/epjd/e2003-00236-0

THE EUROPEAN PHYSICAL JOURNAL D

Stark spectroscopy of high-lying odd parity levels in atomic samarium

T. Kondo[1,a], D. Angom[2,b], I. Endo[2], A. Fukumi[1], T. Horiguchi[3], M. Iinuma[2], and T. Takahashi[2]

[1] Department of Physics, Faculty of Science, Hiroshima University, 1-3-1 Kagamiyama, Higashi-Hiroshima 739-8526, Japan
[2] Graduate School of Advanced Sciences of Matter, Hiroshima University, 1-3-1 Kagamiyama, Higashi-Hiroshima 739-8530, Japan
[3] Department of Clinical Radiology, Faculty of Health Sciences, Hiroshima International University, 555-36 Gakuendai, Kurose, Hiroshima 724-0695, Japan

Received 7 October 2002 / Received in final form 10 February 2003
Published online 30 July 2003 –

Abstract. We have performed a series of experiments to observe 11 Stark-induced E1 transitions from the 15650.55 cm^{-1} level to higher levels with odd parity in samarium (Sm) with optical double-resonance technique. Five Stark-induced E1 transition to the 28233.08, 28613.22, 28913.97, 29041.31 and 29130.03 cm^{-1} levels have been observed. In order to investigate the contributors to the Stark-induced E1 transition, we have measured scalar and tensor polarizabilities for the observed Stark-induced E1 transitions. Clear Stark splittings were observed for the levels 28233.08 and 28613.22 cm^{-1}, and their tensor polarizabilities were determined for each isotope. Scalar polarizabilities were determined for the 28233.08, 28613.22, 28913.97 and 29130.03 cm^{-1} levels for the first time. Among them, scalar polarizability for the 28233.08 cm^{-1} level was the largest in magnitude and was $3.60(10) \times 10^3$ kHz/(kV/cm)^2 for ^{152}Sm. We noticed that both scalar and tensor polarizabilities of the 28233.08 cm^{-1} level depend on the isotope; the difference of magnitude of the scalar and tensor polarizabilities between ^{144}Sm and ^{154}Sm were remarkably large and were about 10 and 6 percent, respectively.

PACS. 32.60.+i Zeeman and Stark effects – 32.10.Dk Electric and magnetic moments, polarizability

1 Introduction

The spectroscopic studies of rare-earth elements have been performed for many decades. On atomic samarium (Sm), in particular, the hyperfine structure (hfs) and isotope shift (IS) were of special interest because of both its large nuclear deformation and complicated electronic structure [1–8]. Several measurements of hfs and IS have been reported on some excited levels as well as those of the ground multiplet [8–11], while there is the limited number of studies on Stark and Zeeman effects.

The Stark effects have been systematically investigated by a group at Hannover [12–15]. They determined the tensor polarizabilities of the levels in the ground multiplet with 5 percent precision with a nonlinear level-crossing technique. The tensor polarizabilities of odd parity levels were measured by using a quantum beat spectroscopy [16]. Fukumi *et al.* also measured tensor polarizabilities with high precision in an atomic-beam laser spectroscopy [17]. Measurements mentioned above are mostly on the odd parity levels below 23000 cm^{-1}, because they are easily excited by a visible photon with E1 transition from the ground state. The studies on Stark effects of high-lying levels above 23000 cm^{-1} have never been reported except for the recent paper [18].

Since the electronic structure of rare-earth elements is very complex, extensive spectroscopic studies are highly desired to check the accuracy of theoretical calculations [19]. Investigation of Stark effects of high-lying levels is necessary also for planning an experiment to study the fundamental symmetry-breaking phenomena in atomic system, such as parity non-conservation (PNC) and electric dipole moment [16]. It is important, for the former, to measure Stark-induced E1 ($E1_{ST}$) transition of each isotope [20]. The spectroscopic studies of high-lying levels of both even and odd parity are insufficient so far. High-lying odd parity levels are difficult to access, while even parity levels are easily accessible. As authors are planning a PNC measurement with two step excitation, the information of high-lying odd parity levels are necessary [18].

A naive idea to study high-lying odd parity levels might be to observe M1 transition from an excited intermediate odd parity level to a higher level with the same parity. This, however, is not practical, because M1 transition is too weak. On the other hand, $E1_{ST}$ transition

[a] e-mail: kondo@photon.hepl.hiroshima-u.ac.jp
[b] *Present address:* Physical Research Laboratory, Navarangpura, Ahmedabad 380 009, India.

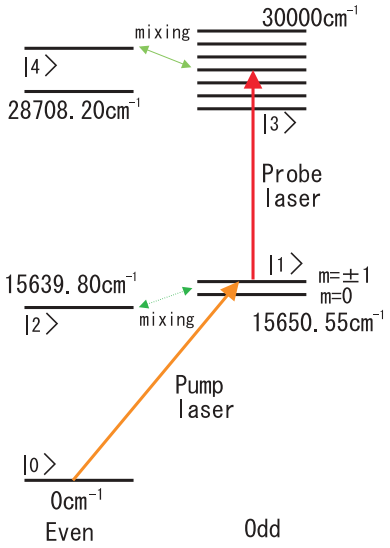

Fig. 1. Level scheme of the Stark spectroscopy setting 15650.55 cm^{-1} level as $|1\rangle$. The pump laser is locked to the transition from 0 cm^{-1} to 15650.55 cm^{-1} with $m = \pm 1$.

under a strong electric field is generally stronger than M1 transition, so that we can study high-lying odd parity levels with the optical double resonance (ODR) of "E1–$E1_{ST}$ transition".

In this paper, we describe a new experiment of ODR spectroscopy on highly excited odd parity levels of atomic Sm. The measured scalar and tensor polarizabilities together with the results of intensity measurements of $E1_{ST}$ transitions are presented.

2 Experiments

2.1 Stark spectroscopy with ODR

For systematic studies of high-lying odd parity levels around 30000 cm^{-1}, we employed ODR technique of "E1–$E1_{ST}$" transition. The relevant level scheme is shown in Figure 1. The Sm atoms in the ground level, even parity level denoted by $|0\rangle$, are excited to the first level $|1\rangle$ by a pump laser. A probe laser excites the atom in $|1\rangle$ to a high-lying odd parity level $|3\rangle$, by $E1_{ST}$ transition. The levels $|2\rangle$ and $|4\rangle$ have even parity and are mixed with $|1\rangle$ and $|3\rangle$, respectively, due to the Stark effect. The frequency of the pump laser is locked to the E1 transition from $|0\rangle$ to $|1\rangle$ so that the population of $|1\rangle$ is kept stable. The $E1_{ST}$ transition from $|1\rangle$ to $|3\rangle$ is observed by sweeping the frequency of the probe laser. The fluorescence emitted from $|3\rangle$ allows us to measure the spectra of high-lying levels with odd parity.

In the level scheme shown in Figure 1, the transition intensity of the $E1_{ST}$ transition, I_{ST}, is expressed as,

$$I_{ST} \propto |\delta_{12}\langle 2|\mathbf{D}|3\rangle + \delta_{34}\langle 1|\mathbf{D}|4\rangle|^2, \quad (1)$$

$$\delta_{ij} = \frac{\langle j|H_{ST}|i\rangle}{E_i - E_j}, \quad (2)$$

Table 1. Second levels which we tried to investigate. The intensities of the fluorescence light from the second level are normalized by the intensities of reference transition from 15650.55 cm^{-1} to 28708.20 cm^{-1} level.

identifier	J	energy (cm^{-1}) [24]	fluorescence intensity
A	2	28065.45	
B	0	28168.22	
C	1	28233.08	0.055(1)
D	2	28359.00	
E	2	28445.02	
F	2	28496.57	
G	1	28613.22	0.096(3)
H	1	28704.25	
I	1	28913.97	0.293(18)
J	2	29041.31	0.035(2)
K	1	29130.03	0.315(13)

where $\mathbf{D}$, δ_{ij}, H_{ST} and E_i are an electric dipole operator, a Stark mixing coefficient, a Hamiltonian of Stark effect and the energy of the ith level, respectively. The $E1_{ST}$-transition amplitude is proportional to both the Stark mixing coefficient and E1 transition; $\langle 2|\mathbf{D}|1\rangle$ and $\langle 1|\mathbf{D}|4\rangle$. For observing the $E1_{ST}$ transition from $|1\rangle$ to $|3\rangle$, one or both of following conditions must be satisfied: one is that δ_{34} and $\langle 1|\mathbf{D}|4\rangle$ are strong. The other is that δ_{12} and $\langle 2|\mathbf{D}|3\rangle$ are strong.

In order to perform the spectroscopy, it is necessary to choose a level with large polarizabilities as the first level $|1\rangle$. Even if unknown Stark effect of the second level $|3\rangle$ be weak, the spectrum would be obtained provided the E1 transition $\langle 2|\mathbf{D}|3\rangle$ is strong. We chose 15650.55 cm^{-1} level with a total electronic angular momentum, $J = 1$, and a magnetic quantum number, $m = \pm 1$, as the level $|1\rangle$ as shown in Figure 1. The polarizabilities of the 15650.55 cm^{-1} level are known to be large [17] and 15639.80 cm^{-1} level may be mixed strongly with it. Another reason for the choice of $|1\rangle$ is that the pair of 15650.55 cm^{-1} and 15639.80 cm^{-1} levels are reported to be mixed each other by PNC Hamiltonian [21]. We chose the levels listed in Table 1 for the present study. The levels with $J = 0$, 1 or 2 are used, because $|1\rangle$ has $J = 1$.

2.2 Apparatus

A schematic view of the experimental layout is shown in Figure 2. A CW tunable ring dye laser (Spectra Physics 380A) pumped by an Ar-ion laser (Spectra Physics 2016) was used to excite atoms to the first level $|1\rangle$. The typical single-mode line width was 40 MHz. The dye used was DCM and the output laser power was typically 50 mW at 5 W pumping. A CW tunable ring titanium-sapphire laser (Coherent CR899-29) pumped by an Ar-ion laser (Coherent INNOVA-310) was used as the probe laser. Its line width and the output power was 500 kHz and about 500 mW at 8 W pumping, respectively.

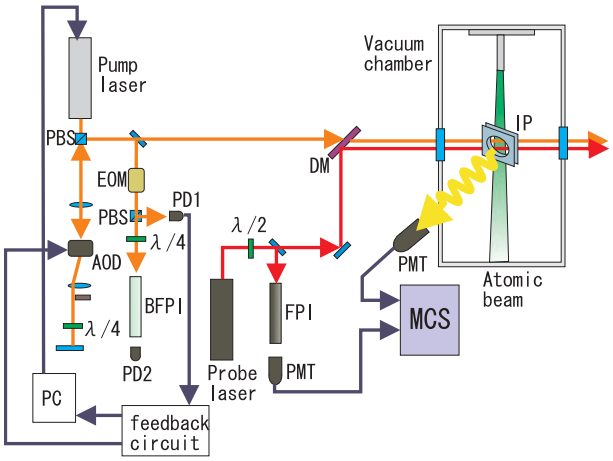

Fig. 2. Overview of the experimental setup. The abbreviations used are as follows; PMT represents a photo-multiplier tube, FPI a Fabry-Perot interferometer, BFPI a Broadband Fabry-Perot interferometer, DM a dichroic mirror, AOD an acousto-optic deflector, EOM an electro-optic modulator, PC a personal computer, PBS a polarized beam splitter, $\lambda/2$ a half-wave plate, $\lambda/4$ a quarter-wave plate, MCS a multi-channel scalar. PD1 and PD2 denote photo-diodes. IP denotes an interaction point.

The pump-laser beam focused by a lens entered a acousto-optic deflector (AOD) after going through a polarization beam splitter (PBS). The first order diffraction beam from the AOD went through a lens and $\lambda/4$ plate and went back along the same way after being reflected by a mirror. After reaching the PBS again, the light beam was bent by 90 degree toward a vacuum chamber. A reference signal for laser-frequency stabilization was taken by a beam sampler before the vacuum chamber.

A large part of the probe-laser beam went through a half wave ($\lambda/2$) plate and reached the vacuum chamber. The direction of the polarization could be adjusted with the $\lambda/2$ plate. A small amount of the probe-laser beam was sampled by a relative frequency-calibration system which consisted of a Fabry-Perot interferometer (FPI) and a photo-multiplier tube (PMT). The pump and probe beams were merged together to follow the same path by a dichroic mirror and led into the vacuum chamber as shown in Figure 2.

We employed an FM sideband method to narrow the laser line-width of the pump laser and resulted in reduced fluctuation of population of the first level. It also suppressed a possible drift away from the resonance condition of the first excitation. A portion of the pump laser passed through an electro-optical modulator (EOM) and reached a broadband Fabry-Perot interferometer (BFPI) through a PBS and a $\lambda/4$ plate. The modulation frequency was 15 MHz. The interference of the leaking and directly reflected lights produced a modulated signal at a photo-diode PD1 to be demodulated by a double balanced mixer (DBM). We used the output signal of the DBM as an error signal for the feedback system. The transmitted light from the BFPI was monitored with a photo-diode PD2. The BFPI was made of super invar and the temperature was controlled to within ± 0.5 °C. The absolute frequency of a longitudinal mode was stable for more than 40 minutes. The lower frequency component of the error signal was digitized by an analog to digital converter and was transmitted to a personal computer (PC). The feedback signal from the PC was sent to the controller of the pump laser through a digital to analog converter to stabilize its frequency drift. The higher frequency component was electrically amplified and fed to the AOD to narrow the line-width of the pump laser to typically 2 MHz. By moving a piezo device attached to one of the mirror of the BFPI, the locking point was adjusted so as to get maximum amount of the fluorescence lights from the 15650.55 cm^{-1} level.

The basic setup of an atomic-beam oven, vacuum system and data-taking system is the same as that described in references [17,18]. The laser lights and the atomic beam crossed perpendicularly to each other at an interaction point (IP), where electrodes made of BK7 coated with ITO ($InSnO_2$) were installed to generate an electric field. They were electrically conductive but optically transparent. The size of the electrode plates were 40 mm in diameter and 2 mm in thickness and the gap between coated surfaces was 8.5 mm. The high voltage was applied to one of the electrodes by a DC-voltage supply and the other was grounded. The direction of the electric field was perpendicular to both the atomic beam and the laser beam. A digital voltmeter and a high-voltage probe measured the voltage applied to the electrodes. A spherical mirror was attached just behind one of the electrodes to collect the fluorescence photons to a PMT installed on the opposite side of the mirror.

The probe-laser system was equipped with a computer controlled wave-meter and the wavelength were monitored with another PC. A TTL gate pulse from the laser controller initiated a frequency sweep. It was, at the same time, transmitted to a CAMAC multi-input level ADC, which was triggered by the same clock generator as the one used for multi-channel scalars (MCSs).

3 Calibration

3.1 Relative frequency

All peaks of the FPI spectrum were fitted with the Gaussian functions and the central channels of the peaks were determined. The FSR has been calibrated to be 300.1±0.3 MHz referring to the hfs splitting of rubidium ^{85}Rb [22]. The MCSs channel was converted to the relative frequency following the same procedure described in reference [10]. A scanning frequency error, $\Delta f_{\rm scan}$, is a standard deviation of the data points from the straight line and is mainly due to a jitter of a laser scan. The value of $\Delta f_{\rm scan}$ was typically 300 kHz.

3.2 Start frequency of the probe laser

While the measurements of tensor polarizability (α_2) require only frequency difference between splitted peaks observed in a single frequency scan, the measurements of

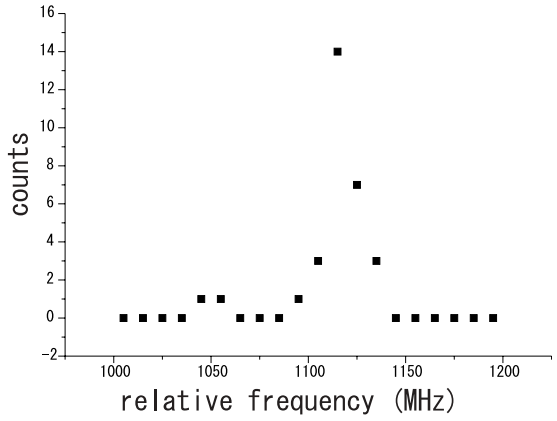

Fig. 3. Distribution of the relative frequency from the leading edge of the TTL logic gate to the center of fluorescence peak. The vertical axis represents the number of occurrence in a 10 MHz bin.

scalar polarizability (α_0) demand the frequency shift of a fluorescence peak relative to an external absolute standard. In order to check if a leading edge of the TTL logic gate can be used as the frequency standard, we measured both the leading edge of the gate-pulse shape and a resonance peak of atoms during the laser scan. The fluorescence peak of the transition of 15650.55 $\text{cm}^{-1} \rightarrow$ 28708.20 cm^{-1} was chosen for this purpose. As the laser frequency during the laser scan is proportional to time, the time difference between the appearance of the leading edge and that of the fluorescence peak is proportional to the relative frequency from the start frequency to the resonance frequency. We measured the leading edge of the gate-pulse shape and the fluorescence peak about 30 times for 40 minutes. The distribution of the relative frequency from the leading edge to the center of the fluorescence peak is shown in Figure 3. The vertical axis represents the number of occurrence in a 10-MHz bin. The observed distribution of the fluctuation was fitted with the Gaussian function and the full width at half maximum (FWHM) was found to be 19.5 MHz.

3.3 Electric field

The electric field at the IP was calibrated by measuring the voltage applied to the electrodes and the Stark splitting of the transition; $4f^6 6s^2\ ^7\text{F}_2$ ($E = 811.92\ \text{cm}^{-1}$) $\rightarrow$ $4f^6 6s6p\ ^7\text{F}_1$ ($E = 13999.50\ \text{cm}^{-1}$), for which the α_2 has been already known [16]. The applied voltage V is proportional to the actual electric field $\mathbf{E}$ and is written as;

$$\mathbf{E} = \frac{V}{d}\hat{\mathbf{e}}, \tag{3}$$

where d and $\hat{\mathbf{e}}$ are the gap of the electrodes and a unit vector directed along the electric field, respectively. The reproducibility of the electric field was confirmed from the repeated measurements. The gap d of 0.8395 ± 0.0079 cm was derived from the measured Stark splitting and applied voltage.

4 Measurements and data analysis

4.1 Basic formula

A mixed level $|nJ\rangle'$ due to the Stark effect is expressed with the first order perturbation theory using a Hamiltonian, $H_{\text{ST}} = -\mathbf{D}\cdot\mathbf{E}$, as

$$|nJ\rangle' = |nJ\rangle + \sum_i \frac{\langle n_i J_i|H_{\text{ST}}|nJ\rangle}{E - E_i}|n_i J_i\rangle. \tag{4}$$

The symbols n and E are a main quantum number and a level energy of $|nJ\rangle$, respectively. The subscript i runs over all possible opposite parity levels to $|nJ\rangle$. The expression of the intensity of the E1_{ST} transition is,

$$I \propto \left|\sum_i \frac{\langle n_i J_i|H_{\text{ST}}|nJ\rangle}{E - E_i}\langle 15650.55|\mathbf{D}|n_i J_i\rangle\right|^2, \tag{5}$$

where $|15650.55\rangle$ corresponds to the first level $|1\rangle$ in Figure 1. This shows that the transition intensity is proportional to $\mathbf{E}^2$.

The energy shift due to an external electric field can be expressed as follows;

$$\begin{aligned} W &= \sum_i \frac{|\langle n_i J_i|H_{\text{ST}}|nJ\rangle|^2}{E - E_i} \\ &= -\frac{1}{2}\left\{\alpha_0(J) + \frac{3m_J^2 - J(J+1)}{J(2J-1)}\alpha_2(J)\right\}\mathbf{E}^2, \end{aligned} \tag{6}$$

where $\alpha_0(J)$, $\alpha_2(J)$ and m_J are a scalar and tensor polarizabilities and magnetic quantum number, respectively.

The mathematical expressions of the $\alpha_0(J)$ and $\alpha_2(J)$ are

$$\alpha_0(J) = -\frac{2}{3(2J+1)}\sum_i A_{J_i}, \tag{7}$$

$$\begin{aligned} \alpha_2(J) = 2&\left\{\frac{10J(2J-1)}{3(2J+3)(J+1)(2J+1)}\right\}^{\frac{1}{2}} \\ &\times \sum_i a_{J_i} A_{J_i}, \end{aligned} \tag{8}$$

$$A_{J_i} = \frac{|\langle n_i J_i||\mathbf{D}||nJ\rangle|^2}{E - E_i}, \tag{9}$$

with

$$a_{J_i} = (-1)^{J+J_i+1}\begin{Bmatrix} J & J & 2 \\ 1 & 1 & J_i \end{Bmatrix}. \tag{10}$$

4.2 Confirmation of the Stark-induced E1 transition

The frequency of the probe laser was swept for 10 GHz, which is much wider than a typical Stark shift, around the energy of the levels listed in Table 1. The fluorescence lights from the second levels with odd parity were selected by an optical filter transparent to a wavelength shorter than 630 nm. It blocked most of the fluorescence

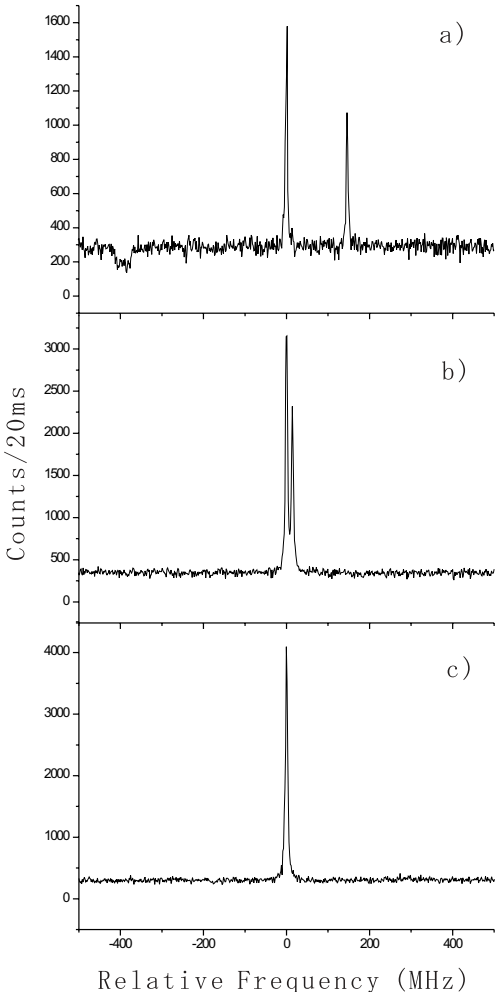

Fig. 4. Typical spectra of the Stark splitting of ^{152}Sm at the electric field of 21 kV/cm. Figures (a), (b) and (c) show the Stark splitting of the level C, G and K, respectively.

lights from the first level and the thermal photons from the atomic-beam oven of which temperature was about 900 °C. To detect the signal of the $E1_{ST}$ transition, the electric field of about 20 kV/cm was applied. As the Stark effect and IS of the first level were well-known [17], we could tune the laser frequency of the pump laser to a resonance frequency of a specific isotope. The probe laser excited Sm atoms from $|1\rangle$ to $|3\rangle$ of the isotope chosen by the pump laser. In this circumstance, the $E1_{ST}$ transitions to the levels C, G, I, J and K shown in Table 1 were observed as clear peaks in the spectra among 11 levels. A typical spectrum of the level C is shown in Figure 4a. The background level was almost constant and typically around 300 counts per 20 ms. It was dominated by the fluorescence lights from the first level because of imperfectness of the optical filter. The hight of the background-subtracted peak was about 1300 counts per 20 ms in the case of ^{152}Sm. The electronic noise was about 20 counts per 20 ms. The FWHM of the peaks, 4 MHz, was consistent with a residual Doppler broadening.

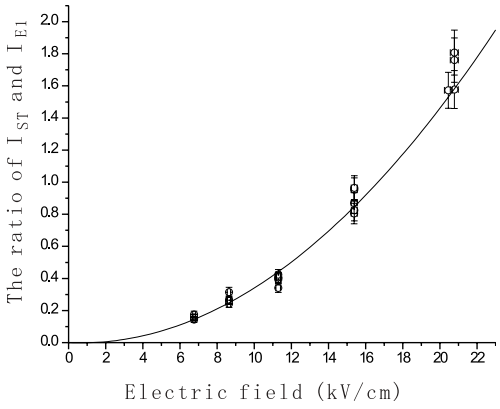

Fig. 5. Plot of the peak intensities, I_{ST}, of the transition from 15650.55 cm^{-1} to 28233.08 cm^{-1} normalized by the E1 intensity, I_{E1}, of the transition from 0 cm^{-1} to 15650.55 cm^{-1} as a function of the electric field.

In order to check that the observed peaks were the signatures of the $E1_{ST}$, we measured $\mathbf{E}^2$ dependence of the peak intensity. In Figure 5, we show, as an example, the observed intensity of the transition to the level C on ^{152}Sm under the electric field varied from 6 to 21 kV/cm. The vertical axis represents the intensities normalized by the fluorescence from the first level. The intensities were fitted with the function of $y(\mathbf{E}) = a\mathbf{E} + b\mathbf{E}^2$, where a and b are fitting parameters. The first term of the fitting function represents a interference of the $E1_{ST}$ amplitude with the M1 or E2. The second term arises from square of the absolute value of the $E1_{ST}$ amplitude. The parameters a and b are found to be $-5.0(22) \times 10^{-3}$ (cm/kV) and $3.9(20) \times 10^{-3}$ (cm/kV)^2, respectively. We notice that the quadratic term is much larger than the linear term at 20 kV/cm. The electric field dependence of the transition intensity to the level G, I and K are shown in Figure 6. Each peak intensity I_{ST} is normalized by the E1 intensity, I_{28708}, of the transition from 15650.55 cm^{-1} to 28708.20 cm^{-1} as a function of the electric field. As the fluorescence peak disappeared when we set $\mathbf{E} = 0$, the peak for J is probably also due to the $E1_{ST}$ transition.

4.3 Fluorescence intensity from the second levels

The factors which affect the intensity of fluorescence light from the second levels are the intensity of atomic beam, the probe and pump laser power, the population of the first level and the detection efficiency. The detection efficiency depends on decay mode and branching. The laser power of the probe and pump laser which went through the vacuum chamber were monitored by a power meter. The stability of the population of the first level and the intensity of the atomic beam could be checked by monitoring the background level due to the fluorescence lights from the first level. The magnitude of fluctuation of the fluorescence lights was about 10 percent.

To confirm the stability of the experimental system related to the intensity measurements, we took a spectrum of the reference E1 transition from the first level to

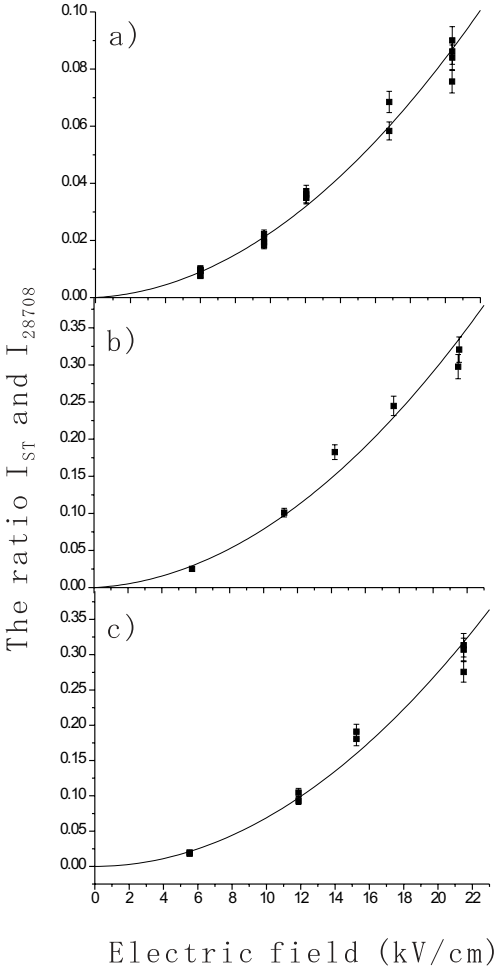

Fig. 6. Plot of the peak intensities, $I_{\rm ST}$, of the transition from 15650.55 cm^{-1} to the G, I and K normalized by the E1 intensity, I_{28708}, of the transition from as a function of the electric field. Figures (a), (b) and (c) are electric field dependence of the $\rm E1_{ST}$ transition to the level G, I and K, respectively.

28708.20 cm^{-1} within one hour before and after the intensity measurements. The reason of taking this transition as the reference is that 28708.20 cm^{-1} level is the nearest one to 28233.08 cm^{-1} level. This transition was also used in last experiments by our group [18]. The optical filter before the PMT was changed to accept the wavelength longer than 660 nm and the frequency region of the probe laser was changed leaving other conditions fixed. The intensities of fluorescence from the second levels observed at the electric field of 21.6 kV/cm are shown in Table 1. Each intensity was normalized by that of the reference E1 transition. We notice that the transition to the level I and K are bigger than others by one order of magnitude. This feature may be due to either large $\rm E1_{ST}$ transition of the I and K or their decay branching favorable to fluorescence detection by the PMT.

Table 2. Obtained values of the α_0 and α_2 for each second level.

levels	isotope	α_0 (kHz/(kV/cm)^2)	α_2 (kHz/(kV/cm)^2)
C	^{144}Sm	$4.11(16) \times 10^3$	$-201.3(15)$
	^{148}Sm	$3.89(9) \times 10^3$	$-205.6(18)$
	^{150}Sm		$-208.2(16)$
	^{152}Sm	$3.60(10) \times 10^3$	$-212.7(17)$
	^{154}Sm	$3.69(9) \times 10^3$	$-214.0(17)$
G	^{144}Sm		$-20.74(23)$
	^{148}Sm		$-19.99(18)$
	^{150}Sm		$-20.86(20)$
	^{152}Sm	$-5.3(109) \times 10^1$	$-20.49(22)$
	^{154}Sm		$-19.76(19)$
I	^{152}Sm	$-1.4(16) \times 10^2$	$< \lvert 6.47(19) \rvert$
J	^{152}Sm		$< \lvert 5.77(15) \rvert$
K	^{152}Sm	$-3.4(12) \times 10^2$	$< \lvert 5.47(14) \rvert$

4.4 Tensor polarizability α_2

We investigated the Stark splitting for observed five $\rm E1_{ST}$ transition to the level C, G, I, J and K. In order to measure the Stark splitting on ^{152}Sm, the electric field of about 21 kV/cm was applied. We found the clear and wide splitting of the level C as shown in Figure 4a, while for the level G, the splitting was small, see Figure 4b. We could not find obvious splitting for the levels K, I nor J. The spectrum of the level K is shown in Figure 4c. To obtain energy splitting and tensor polarizability, the two peaks of the level C and G were fitted with two Lorentzian functions. The peak for the levels I, J and K was fitted with one Lorentzian function and its FWHM gave us the upper limit of their tensor polarizabilities. The Levenberg-Marquardt method was used for the Lorentzian fitting to the background-subtracted atomic spectra in order to obtain the central frequency of the peak and its statistical error $\Delta f_{\rm stat}$.

The tensor polarizabilities were derived from the Stark splitting, ΔW, of the second level as,

$$\alpha_2(J=1) = -\frac{2}{3}\frac{\Delta W}{\mathbf{E}^2}. \qquad (11)$$

The error of α_2 depends on $\Delta f_{\rm scan}$, $\Delta f_{\rm stat}$, the ambiguity from the error of the FSR, $\Delta f_{\rm FSR}$, and the error of gap of the electrodes, Δd, described in Section 3.3. The typical magnitude of $\Delta f_{\rm scan}$, $\Delta f_{\rm stat}$ and $\Delta f_{\rm FSR}$ were 300 kHz, 100 kHz and 100 kHz, respectively. The uncertainty of d was about 0.94 percent and dominated the error of α_2. Note that ΔW is only due to the α_2 of the second level, because only one of the sub-levels in the first level is populated by the pump laser.

The α_2 for several isotopes (^{144}Sm, ^{148}Sm, ^{150}Sm, ^{152}Sm, ^{154}Sm) was measured for both the levels C and G. The obtained α_2 of each energy level is listed in Table 2. Typical spectra of the transition to the level C for two isotopes, ^{144}Sm and ^{154}Sm, are shown in Figure 7. One can

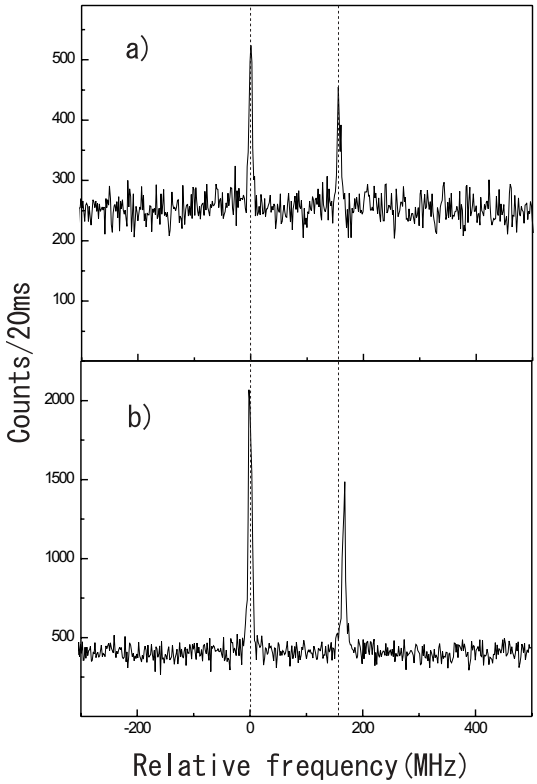

Fig. 7. Stark splittings of 28233.08 cm^{-1} level at the electric field of 22.73 kV/cm for ^{144}Sm and ^{154}Sm are shown in (a) and (b), respectively.

see the difference of the Stark splittings between them. The tensor polarizability α_2 is negative and its absolute value is increasing with the mass number. The difference of the magnitude of α_2 between ^{144}Sm and ^{154}Sm is as large as about 6 percent.

4.5 Scalar polarizability α_0

The Stark shifts of the level C, G, I and K were measured to determine α_0. Typical spectra of the Stark shift of the level C for various electric field are shown in Figure 8, where the quoted frequencies are relative to the start frequency denoted by $f_{\rm const}$. The α_0 of the second level can be derived from an external field dependence of the shift of the peak. Note that the observed energy shift is sum of the energy shift of the first level W_1 and that of the second level. The energy shift of the center of gravity, f_c, of the second levels is expressed as,

$$f_c = f_{c2nd} + W_1 = -\frac{1}{2}\alpha_0 \mathbf{E}^2 + f_{\rm const},$$
$$f_{c2nd} = \{f(m=0) + \frac{2}{3}(f(|m|=1) - f(m=0))\} \quad (12)$$

where $f(m)$ is the measured energy shift and the central frequency of the peak with m relative to the start frequency. The energy shift of the sub-level with $|m| = 1$, W_1, was estimated with the known values of α_2 (Tab. 5 of Ref. [17]) and α_0 (=−999(80) kHz/(kV/cm)^2 from Ref. [23]). The plot of f_c as a function of the squared electric field is shown in Figure 9. The free parameters α_0 and $f_{\rm const}$ were determined by fitting the function (Eq. (12)) to the experimental data.

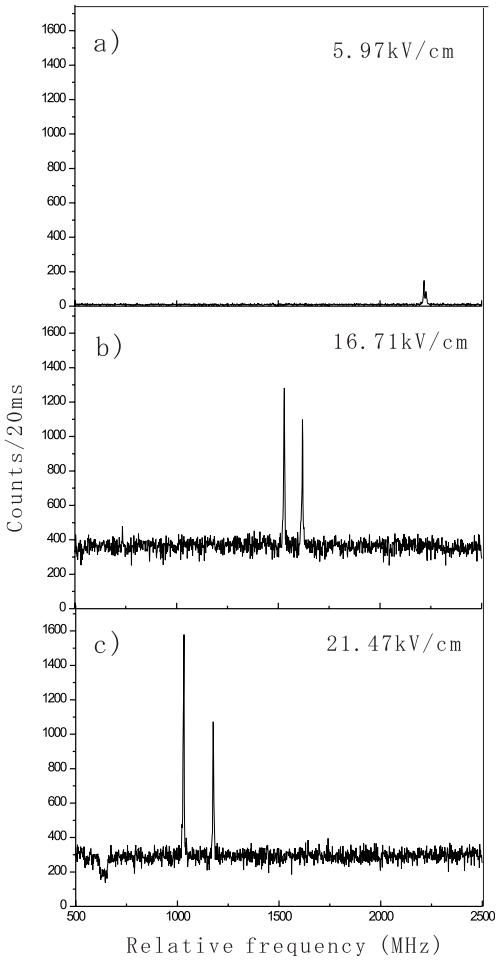

Fig. 8. Stark shifts of the 28233.08 cm^{-1} level on ^{152}Sm. Figures (a), (b) and (c) show the Stark shift at the electric field of 5.97 kV/cm, 16.71 kV/cm and 21.47 kV/cm, respectively.

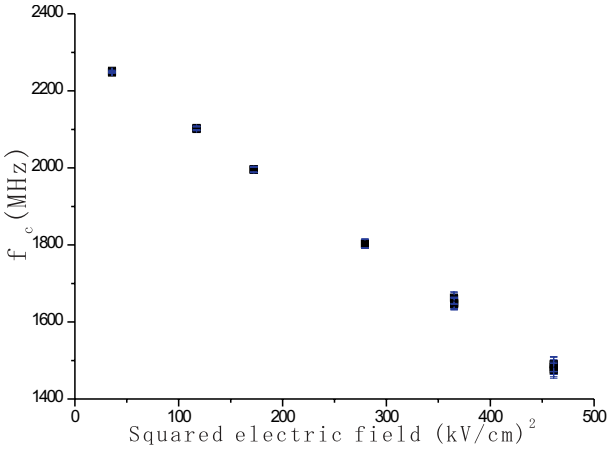

Fig. 9. Plot of the f_c with respect to the squared electric field.

We measured the α_0 for several isotopes (^{144}Sm, ^{148}Sm, ^{152}Sm, ^{154}Sm) on the level C. For other transitions, the α_0 was measured only for ^{152}Sm. Immediately before and after the measurements for each isotope, the control measurements including the calibration process of the electric field were carried out. The obtained α_0 of each energy level is listed in Table 2. The scalar polarizabilities α_0 are positive and decrease with the mass number; the α_0 of ^{144}Sm is 10 percent higher than that of ^{154}Sm. This is the first observation of isotope dependence of the α_0. The error is dominated by the error of α_0 of the first level and that of the start frequency as estimated in Section 3.2.

5 Discussion

5.1 Coefficients of the Stark mixing between 28233.08 cm^{-1} and 28708.20 cm^{-1} level

If either α_0 or α_2 is known, we can estimate the Stark mixing coefficient under the assumption that only one level is mixed with the level of interest [16]. Fukumi *et al.*, for example, determined the Stark mixing coefficient between the level C and 28708.20 cm^{-1} level to be $1.499(16)\times10^{-4}$ (cm/kV) from the measured α_2 of the level C [18] in our last experiments. This estimation is consistent with the present results, that is $1.497(6)\times10^{-4}$ (cm/kV), under the same assumption.

If the one level mixing is assumed, the ratio α_0/α_2 of the level C is expressed as

$$\frac{\alpha_0}{\alpha_2} = -\frac{1}{3}\frac{(-1)^{J_i}}{\begin{Bmatrix}1 & 1 & 2\\ 1 & 1 & J_i\end{Bmatrix}} \qquad (13)$$

from equations (7, 8). For J_i =0, 1 and 2, this ratio is -1, 2 and -10, respectively. None of these values is compatible with the experimental one; $\alpha_0/\alpha_2 = -18.1(3)$ derived from Table 2, where a weighted average with respect to the mass number is adopted in the derivation of it. This means that the approximate method with one level mixing is not good. It is natural to consider that there are many even parity levels which contribute to the polarizabilities. The density of even parity levels at these higher energies is probably comparable to the odd parity levels and it will not be possible to assign real Stark mixing coefficients for each of the multiple possible levels such as Sm atoms. However, as effective mixing coefficients can be expressed as a weighted average by inverse of the energy separation, we can consider dominant levels which contributs to the mixing coefficintes because of their energitical closeness.

Let us, then, discuss about the case of a mixing of dominant two levels. As we measured both the α_0 and α_2, we can solve equations (7, 8) to obtain A_{J_i} and $A_{J_{i'}}$, if there are only two dominant levels (i, i'). Possible combinations of total electronic angular momenta (J_i, $J_{i'}$) are (1, 0), (1, 2) and (0, 2).

Assigning the 28708.20 cm^{-1} level ($J = 1$) to the level with $J_i = 1$, we estimate the Stark mixing coefficients of the level C with 28708.20 cm^{-1} level as $2.242(19)\times10^{-4}$ and $3.659(46)\times10^{-4}$ (cm/kV), for the case that another mixing level has $J_{i'} = 0$ and $J_{i'} = 2$, respectively. In both cases, the present analysis results in about 1.5∼2.4 times lager Stark mixing coefficients than our previous estimation described in reference [18].

5.2 Isotope dependence

The first report on the isotope dependence of α_2 was published by Fukumi *et al.* showing that α_2 of ^{144}Sm differs from that of ^{154}Sm by 0.5 percent [17]. This feature can be explained by following consideration. Assuming that the matrix element $\langle 15650.55|\mathbf{D}|15639.80\rangle$ is equal for all isotopes, the difference of isotope shift, d(ΔE), is estimated by;

$$|\mathrm{d}(\Delta E)| = \left|\frac{\mathrm{d}\alpha_2}{\alpha_2}\Delta E\right| \simeq 2.0 \text{ GHz},$$

where ΔE and dα_2 are the energy spacing of the two levels and the difference of the α_2 in isotopes, respectively. As the transition isotope shift between ^{154}Sm and ^{144}Sm from the ground level to 15650.55 cm^{-1} level was found to be about 8 GHz, about 10 GHz isotope shift of the parity partner, 15639.80 cm^{-1} level, reported in reference [25] would be reproduced by the estimated value of d(ΔE). In this case, it was thus possible to explain the isotope dependence in a simple model.

In the case of the present experiments, however, the observed isotope dependence is about 10 times lager, while the energy of the nearest parity partner, 28708.20 cm^{-1} level, is 44 times more distant compared to the above case. This suggests that the simplified analysis as shown above is not applicable. In order to understand mechanism of the large isotope dependence, more spectroscopic studies on the opposite parity levels including a search for unknown nearby levels are necessary.

6 Conclusion

We performed the experiments to observe 11 Stark-induced E1 transitions from the 15650.55 cm^{-1} level to the higher levels with odd parity in Sm with the optical double-resonance technique. Clear fluorescence peaks were observed for the transition to the 28233.08, 28613.22, 28913.97, 29041.31 and 29130.03 cm^{-1} levels, while for other transitions, we could not identify clear peaks. The fluorescence intensity normalized by that of the reference E1 transition suggests that the transitions to the 28913.97 and 29130.03 cm^{-1} levels are much stronger than others.

We measured the α_0 and α_2 for the observed Stark induced E1 transitions. The clear Stark splittings were observed for the levels, 28233.08 and 28613.22 cm^{-1}, and their α_2 are determined for each isotope. The scalar polarizabilities α_0 were determined for the 28233.08, 28613.22, 28913.97 and 29130.03 cm^{-1} levels for the first time.

Among them, the α_0 for the 28233.08 cm^{-1} level was the largest in magnitude.

Both the α_0 and α_2 of the 28233.08 cm^{-1} level were found to depend on the isotope; the differences of magnitude of the α_0 and α_2 between ^{144}Sm and ^{154}Sm were about 10 and 6 percent, respectively. It is to be noted that the present work is the first report on the isotope dependence of the α_0. As the observed isotope dependence of the α_0 and α_2 are so large that a simple explanation given in the previous paper [17] is not applicable: more experimental data and rigorous analyses are necessary to understand these features.

This work was supported in part by the Matsuo Foundation. One of the authors, A.F., would like to thank the Research Fellowship of the Japan Society for the Promotion of Science for Young Scientists. One of the author, A.D., would like to thank the Japan Society for the Promotion of Science for the Post-Doctoral Fellowship.

References

1. L. Jia, C. Jing, Z. Zhou, F. Lin, J. Opt. Soc. Am. B **10**, 1317 (1993)
2. H. Brand, B. Seibert, A. Steudel, Z. Phys. A **296**, 281 (1980)
3. W.H. King, J. Phys. B: At. Mol. Phys. **14**, 721 (1981)
4. C.W.P. Palmar, D.N. Stancey, J. Phys. B: At. Mol. Phys. **15**, 997 (1982)
5. J. Bauche, R.-J. Champeau, C. Sallot, J. Phys. B: At. Mol. Phys. **10**, 2049 (1977)
6. J.A. Griffith, G.R. Isaak, M.P. Ralls, C.P. van Zyl, J. Phys. B: At. Mol. Phys. **12**, 1 (1979)
7. R. New, J.A.R. Griffith, G.R. Isaak, M.P. Ralls, J. Phys. B: At. Mol. Phys. **14**, 135 (1981)
8. W.G. Jin, T. Horiguchi, W. Yang, I. Endo, Phys. Rev. A **49**, 4398 (1994)
9. M. Wakasugi, T. Horiguchi, W.G. Jin, H. Sakata, Y. Yoshizawa, J. Phys. Soc. Jpn **59**, 2700 (1990)
10. T. Kobayashi, I. Endo, A. Fukumi, T. Horiguchi, Y. Ishida, T. Kondo, T. Kuwamoto, N. Minamoto, T. Nakamura, T. Takahashi, Z. Phys. D **39**, 209 (1997)
11. W.J. Childs, L.S. Goodman, Phys. Rev. A **6**, 2011 (1972)
12. P. Kulina, R.-H. Rinkleff, Z. Phys. A **321**, 15 (1985)
13. C. Neureiter, R.-H. Rinkleff, L. Windholz, J. Phys. B **19**, 2227 (1986)
14. R.-H. Rinkleff, A. Steudel, K. Zeiske, Z. Phys. D **18**, 101 (1991)
15. R.-H. Rinkleff, F. Thorn, Z. Phys. D **32**, 173 (1994)
16. S. Rochester, C.J. Bowers, D. Budker, D. DeMille, M. Zolotorev, Phys. Rev. A **59**, 3480 (1999)
17. A. Fukumi, I. Endo, T. Horiguchi, Y. Ishida, T. Kondo, T. Kuwamoto, H. Matsuzaki, T. Nakamura, T. Takahashi, Z. Phys. D **42**, 243 (1997)
18. A. Fukumi, D. Angom, I. Endo, T. Horiguchi, M. Iinuma, T. Kondo, T. Takahashi, J. Phys. Soc. Jpn **71**, 2137 (2002)
19. A. Dilip, I. Endo, A. Fukumi, M. Iinuma, T. Kondo, T. Takahashi, Eur. Phys. J. D **14**, 271 (2001)
20. V.A. Dzuba, V.V. Flambaum, I.B. Khriplovich, Z. Phys. D **1**, 243 (1986)
21. T.A. Gongora, P.G.H. Sandars, J. Phys. B **19**, 291 (1986)
22. G.P. Barwood, P. Gill, W.R.C. Rowley, Appl. Phys. B **53**, 142 (1991)
23. D. Burow, R.-H. Rinkleff, Arab. J. Sci. Engineer. **17**, 287 (1992)
24. W.C. Martin, R. Zalubas, L. Hagan, *Atomic Energy Levels-The Rare Earth Elements* (National Bureau of Standards, Seattle: Pb, DC, 1978)
25. I.O.G. Davies, P.E.G. Baird, J.L. Nicol, J. Phys. B **21**, 3857 (1988)